Shear-layer structures in near-wall turbulence

By A. V. Johansson[1], P. H. Alfredsson[1], and J. Kim[2]

The structure of internal shear layer observed in the near-wall region of turbulent flows is investigated by analyzing flow fields obtained from numerical simulations of channel and boundary-layer flows. It is found that the shear layer is an important contributor to the turbulence production. The conditionally averaged production at the center of the structure was almost twice as large as the long-time mean value. The shear-layer structure is also found to retain its coherence over streamwise distances on the order of a thousand viscous length units, and propagates with a constant velocity of about 10.6 u_τ throughout the near wall region.

1. Introduction

The formation and evolution of shear-layer-like structures in the near-wall region of turbulent flows have been recognized to be intimately coupled to turbulence production. Most of the information on these structures has been obtained from flow visualizations, although probe measurements have provided a limited quantitative information. Computer-generated data bases, obtained from numerical simulation of turbulent flows which contain velocities and pressure fields in three-dimensional space and time, make it possible to study these structures in more detail, especially regarding their space-time evolution.

The main body of the results presented here has been obtained from simulation data for turbulent channel flow at a Reynolds number of 180 (based on half-channel height and the friction velocity) with a grid of $128 \times 129 \times 128$ points. The grid spacing in terms of viscous units was 17.7 in the streamwise and 5.9 in the spanwise direction.*

Very strong and dynamically important (for the process of turbulence production) shear-layers have been shown to exist in the buffer region of near-wall turbulent flows, and are related to the lift-up of low-speed streaks from the viscous sublayer. A characteristic feature of these shear layers is, by definition, a high value of the instantaneous velocity gradient $\partial u/\partial y$, but since these structures become highly inclined due to the mean shear, the streamwise velocity gradient ($\partial u/\partial x$) across the shear-layer also becomes large. In experimental investigations, a fixed observer

1 Department of Mechanics, The Royal Institute of Technology, S-10044 Stockholm, Sweden.
2 NASA-Ames Research Center.

* x, y, and z denote the streamwise, normal, and spanwise coordinates normalized by the viscous length scale. Similarly, u, v, and w denote the corresponding fluctuating parts of the velocity normalized by the friction velocity u_τ. Also, other quantities are normalized by viscous scales unless stated otherwise explicitly.

will see a high value of the temporal derivative of the streamwise velocity and a large change in u as the shear-layer passes by. This feature is utilized in the so-called VITA (variable interval time averaging) technique which has been used in various experimental investigations (see, Blackwelder & Kaplan, 1976, and Johansson & Alfredsson, 1982, for example) to detect shear-layer structures in boundary layers and channel flows. With this detection scheme, an event is considered to occur when the variance of u averaged over a "short" time T exceeds a chosen threshold level, k, times the long-time- averaged variance (i.e., u^2_{rms}). The detection position is normally chosen in the buffer region. In the analysis of computer-generated data bases, a spatial counterpart, VISA, is used, where the averaging length will be denoted as L (see Kim, 1985). In the present study, this method was extended by an event-centering technique (see Section 2).

Results for the channel-flow case will be presented in Section 2 concerning the three-dimensional spatial structure of the internal shear layer as well as their propagation characteristics and their development in time. These results will be compared with previously published data obtained from the Göttingen oil channel (Johansson, Alfredsson & Eckelmann, 1987) for a comparable Reynolds number. Comparisons concerning frequency of occurrence of shear-layer structures will also be made with hitherto unpublished oil-channel data by Johansson, Alfredsson & Eckelmann. In Section 3, some results from turbulent boundary-layer flow at two different Reynolds numbers will also be presented. A short summary and conclusions are given in Section 4.

2. Channel-flow results

The first step in the detection of shear-layer structures in the buffer region was to compute the locally averaged variance (or VISA-variance) for various xz-planes. For the following channel-flow results, the detection was applied at $y = 15$ with a threshold level (k) of 1.0. The resulting regions of high variance, indicating the existence of strong shear layers, give a spatially spotty picture (Fig. 1). In Fig. 1 the variance was averaged over 11 grid points in the x-direction, corresponding to about 200 viscous length units, and about 30 regions with levels above 1.0 can be observed. In the present approach, these regions were identified, i.e., their maxima were located and followed from their formation to their disappearance for a time sequence of 141 viscous time units (t_*). Each time step was separated by three viscous time units.

As examples, the space-time history of three high-variance islands marked by A, B, and C in Fig. 1 is shown in Fig. 2, where consecutive plots are separated by $12t_*$. Event C is here followed over more than $70t_*$, during which it has traveled approximately 900 viscous units, corresponding to 5 channel half-heights. However, the shear layer can be identified over considerably larger distances. The mean survival time of the shear layers, such as those indicated in Fig. 1, was approximately $50t_*$, but some strong shear layers could be followed throughout the entire extent of the time studied ($141t_*$).

If the events in Fig. 1 and those detected at $y = 15$ near the opposite wall are divided into intervals of the maximum variance amplitude, the low amplitude will

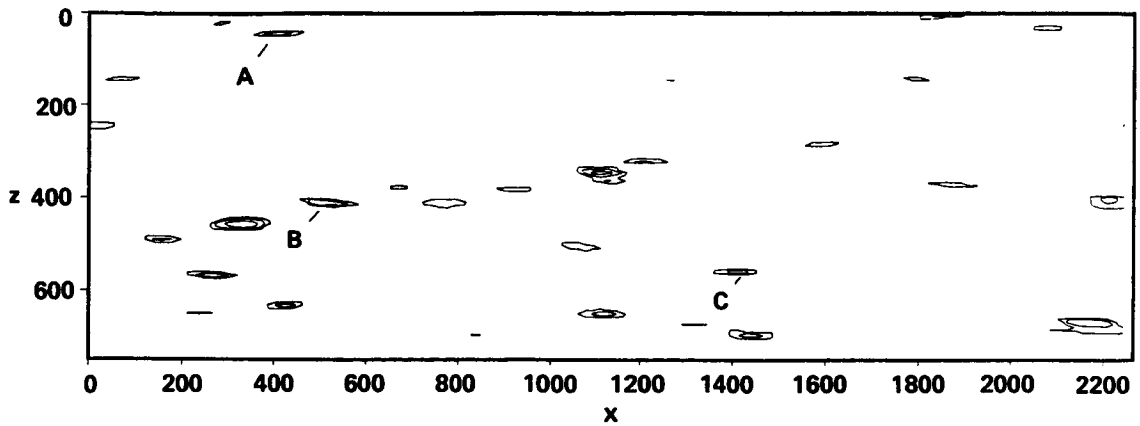

FIGURE 1. Contours of the streamwise velocity variance averaged over a distance of 200 viscous length units at y=15. Contours start at 1.0 with an increment of 0.5.

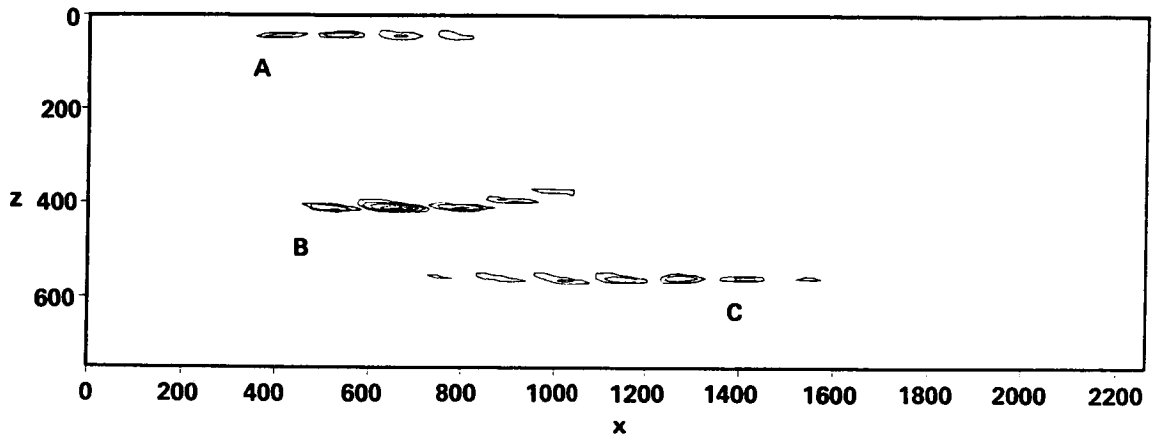

FIGURE 2. The space-time development of the variance associated with the events marked A, B and C in Fig. 1. Time separation between plots is 12 viscous time units.

dominate: i.e., at a given time there are many events (regions of high variance) with a maximum variance just above the threshold. This is illustrated by the open symbols in Fig. 3. On the other hand, if all these events are traced in time to locate the time at which the shear layer is strongest, i.e., the time for which the event has its largest variance amplitude, the picture becomes different (+ symbols in Fig. 3). The most probable variance maximum is now found in the interval 1.5 – 2.0, and values close to 3.5 were observed.

The propagation velocity of the shear layers could be determined (see Fig. 4) from their space-time history, and was found to be 10.6 with a standard deviation of ± 1.0. This is substantially lower than the value 13.0 obtained from an experimental investigation (Johansson, Alfredsson & Eckelmann, 1987) at about the same Reynolds number (10 % higher). In that study, the VITA-detection was carried out

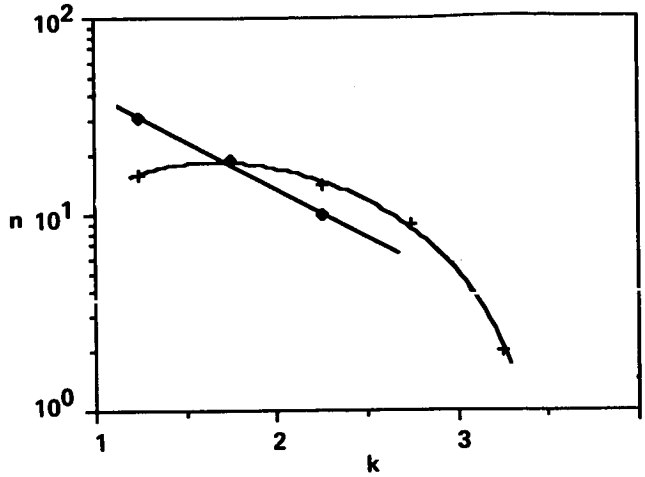

FIGURE 3. Variance amplitude distribution of the events in Fig. 1 (also included are the events detected at the opposite side of the channel: ◇, the amplitude at the time of detection, +, the maximum amplitude of each event when followed over its life-cycle.

at $y = 15$, and a second probe was positioned at various y and x-positions downstream of the detector probe (e.g., at $y = 20$). However, the averaging time was $10t_*$, which would correspond to a shorter averaging length than that used in the present analysis of the numerical data. Also, there is an inherent difference between spatial and temporal data evaluation.

The significance of these flow structures for the flow dynamics in the near-wall region depends on their frequency of occurrence (or probability to occur within a given area). In order to enable comparisons with experimental results obtained with a stationary probe, the average number of detections per z-position was determined and normalized by the streamwise extent of the domain (2260) divided by the propagation velocity (10.6). This means that a shear layer, if signified by a region of high variance extending over several z-positions, gets counted several times, but gives the equivalent of the number of detections per unit time for a fixed probe. Also, the averaging length was converted to an equivalent averaging time by use of the propagation velocity. The agreement is excellent (see Fig. 5) between the present results obtained in this manner and the experimental results (unpublished results by Johansson, Alfredsson, & Eckelmann). One should bear in mind that the scaling used here is immaterial, since the Reynolds number is approximately the same for the two sets of data.

Johansson, Alfredsson & Eckelmann (1987) studied the spatial structure in the symmetry plane of the shear layers. Their results are shown in Fig. 6, where contour lines of the streamwise disturbance velocity normalized with the local rms-value are plotted in the xy-plane. These results may be compared with the corresponding results (Fig. 7a) obtained from the computer-generated data base for channel flow.

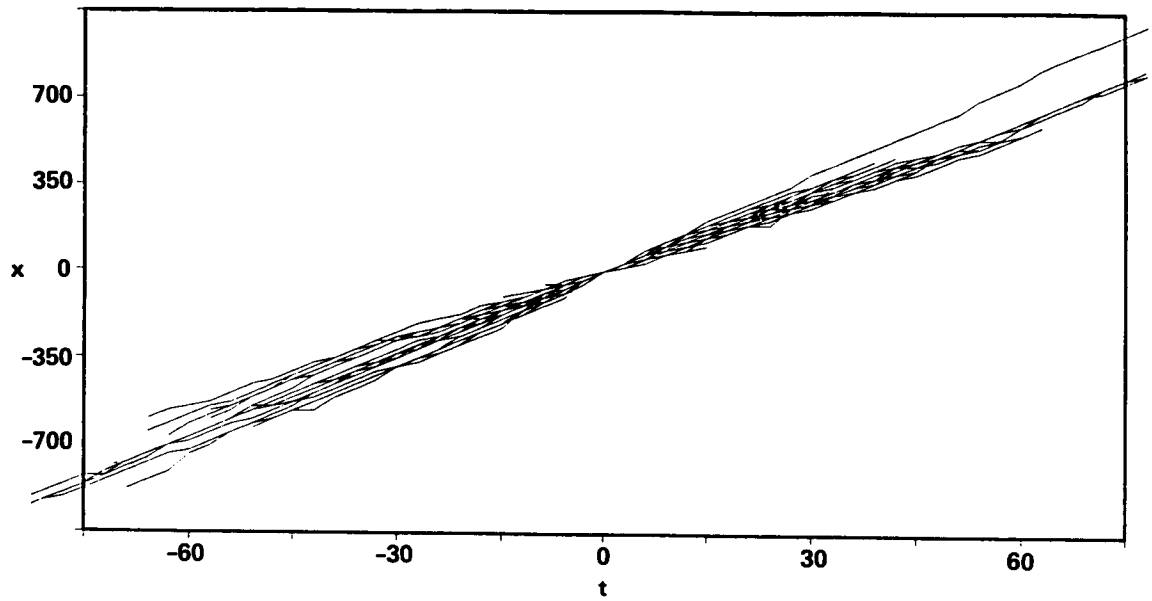

FIGURE 4. Streamwise position of the maximum variance as fuction of time for 60 diffrent events. The plot is centered around the maximum value of the variance for each event. The slope of these lines gives the propagation velocity of the shear layers.

Note that the same contour levels are used in Figs. 6 and 7a. An ensemble average of 60 events detected at both sides of the channel at one time-step are shown. The ensemble averaging here involves centering of the individual realizations in both the x (as in conventional conditional averaging) and the z-direction. Hence, boxes 600 long, 200 wide, and 180 high (the entire half-channel height) in viscous units centered around the point of maximum variance (at $y = 15$) are averaged. The agreement between the experimental and simulation data is seen to be good. In the following, conditional averages (denoted by $< >$) will be presented in absolute scale, i.e., normalized by u_τ (or other appropriate viscous scales).

Figs. 7b and c show the conditionally averaged u and v in the xy-plane. An interesting feature is that, close to the wall, the lifted low-speed fluid is pushed back towards the wall, resulting in a so-called wall-ward interaction. It is also quite evident that there is strong streamwise shear associated with the detected structure and that the regions of coherent velocity are confined below $y \approx 50$. The corresponding results in the xz-plane for $y = 15$ are shown in Fig. 8. The spanwise scale of the primary low- and high-speed regions is seen to be about 50, which is the same as the distance between high- and low-speed streaks in the viscous sublayer. The maximum deviation from the long-time mean in the low- speed region in Fig. 8a is almost twice as large as on the high-speed side of the shear layer. Similarly, the amplitude of the normal velocity is also much higher on the downstream side, which also gives a strong uv-peak in that region (Fig. 8c). The uv-contribution on the sweep side is practically negligible at this y-location.

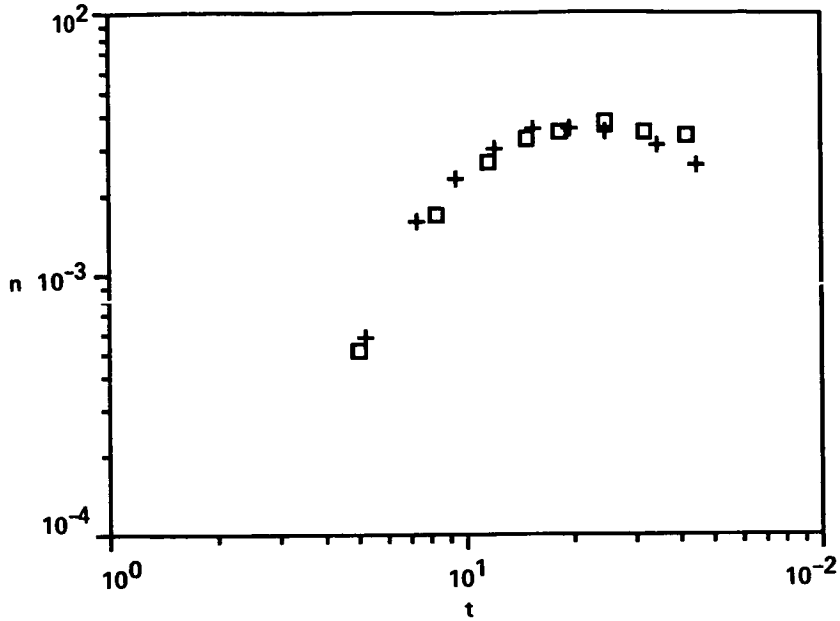

FIGURE 5. Number of events that would be detected per unit time by a stationary probe. Simulation (□) and measurements in the Göttingen oil channel (+) at about the same Reynolds number.

It was found that spanwise centering of the events is essential to obtain reasonable quantitative estimates of the associated Reynolds stress contributions, as is illustrated by Figs. 9a,b. In the latter, no such centering was applied, and the resulting maximum uv is drastically reduced on the ejection side. It should be noted that (to the present authors' knowledge) all previous results, experimental as well as numerical, presented in the literature have been obtained without spanwise centering. The reduction with no spanwise centering can be attributed to the resulting jitter in the spanwise separation between the uv-peak and the detector position, and the fact that the spanwise scale of the uv-peak is rather small.

In conventional conditional averaging procedures, with or without spanwise centering, symmetric patterns are the result of homogeneity of the flow in the spanwise direction. Instantaneous shear-layer structures, on the other hand, often tend to develop strong asymmetries as they propagate downstream. This can give large values of the spanwise gradient of the streamwise velocity at the center of the shear layer. The average of the (absolute) spanwise gradient at the detection point for the events shown in Figs. 7 and 8 was found to be about 0.20 of the mean gradient at the wall, or 2/3 of the local mean gradient. In reality, it is more likely to find an asymmetric structure than the symmetric pattern in Fig. 8a. In order to retain the spanwise asymmetry, often found in the individual events and also in the conditional average, an asymmetry was imposed by switching the z-coordinate according to the sign of the spanwise gradient at the detection point (Fig. 10). The resulting averages illustrate a mechanism for creation of high streamwise gradients

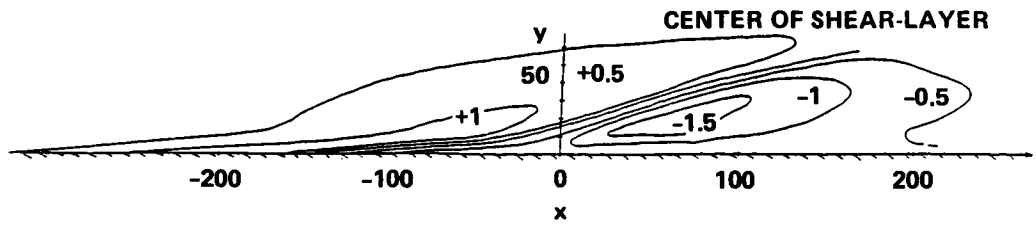

FIGURE 6. Conditionally averaged shear-layer structure in the near wall region in channel flow at Re=200 (Johansson, Alfredsson & Eckelmann, 1987) showing streamwise velocity disturbance ($< u > /u_{rms}(y)$) in the symmetry plane. Events detected by VITA with T^+=10 and k=1.

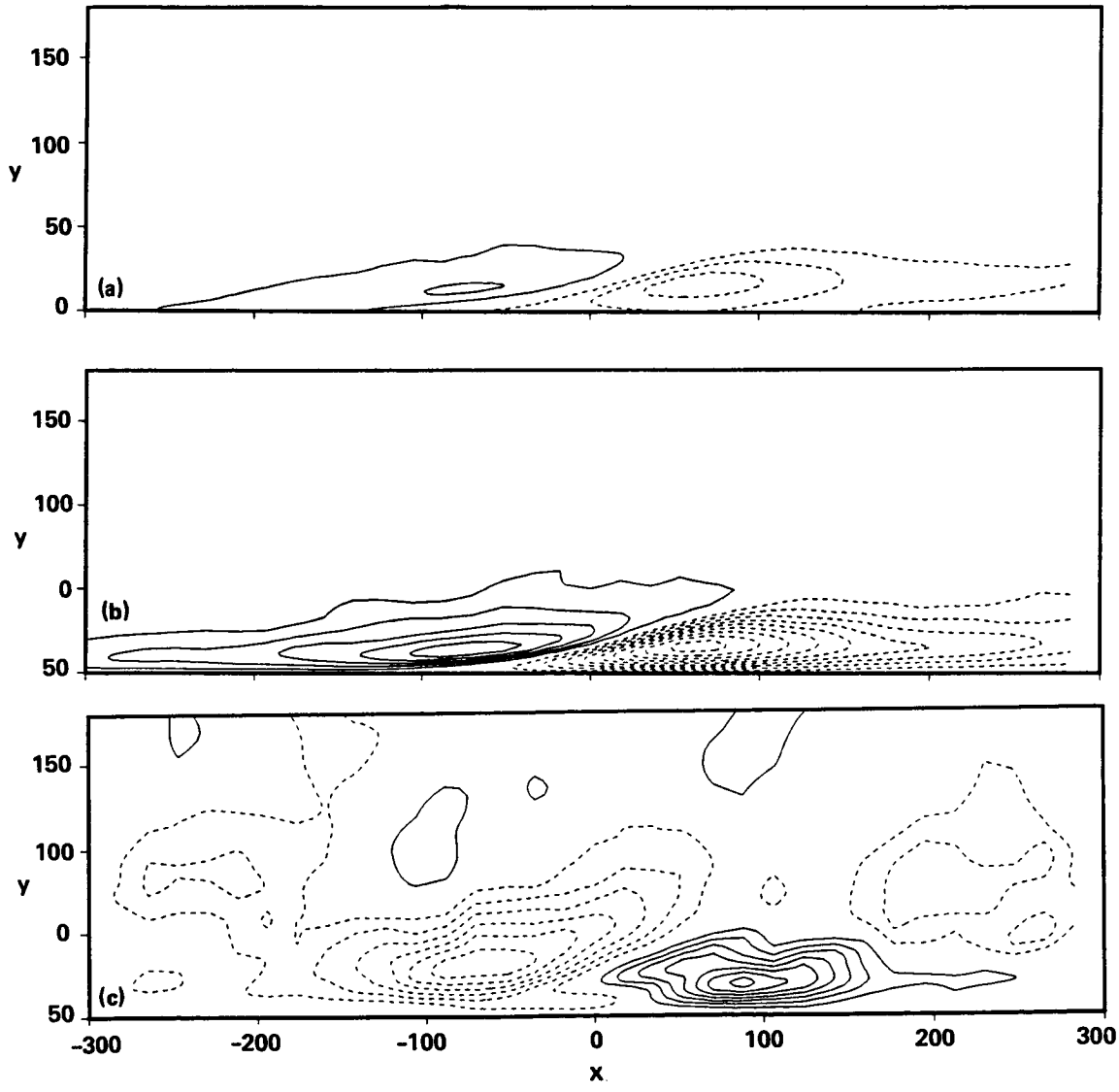

FIGURE 7. Ensemble averaged VISA-events detected with L=200 and k=1. Full drawn lines and broken lines denote positive and negative contours, respectively. (a) $< u > /u_{rms}(y)$, contour increment is 0.5. (b) $< u >$, contour increment is 0.5. (c) $< v >$, contour increment is 0.1.

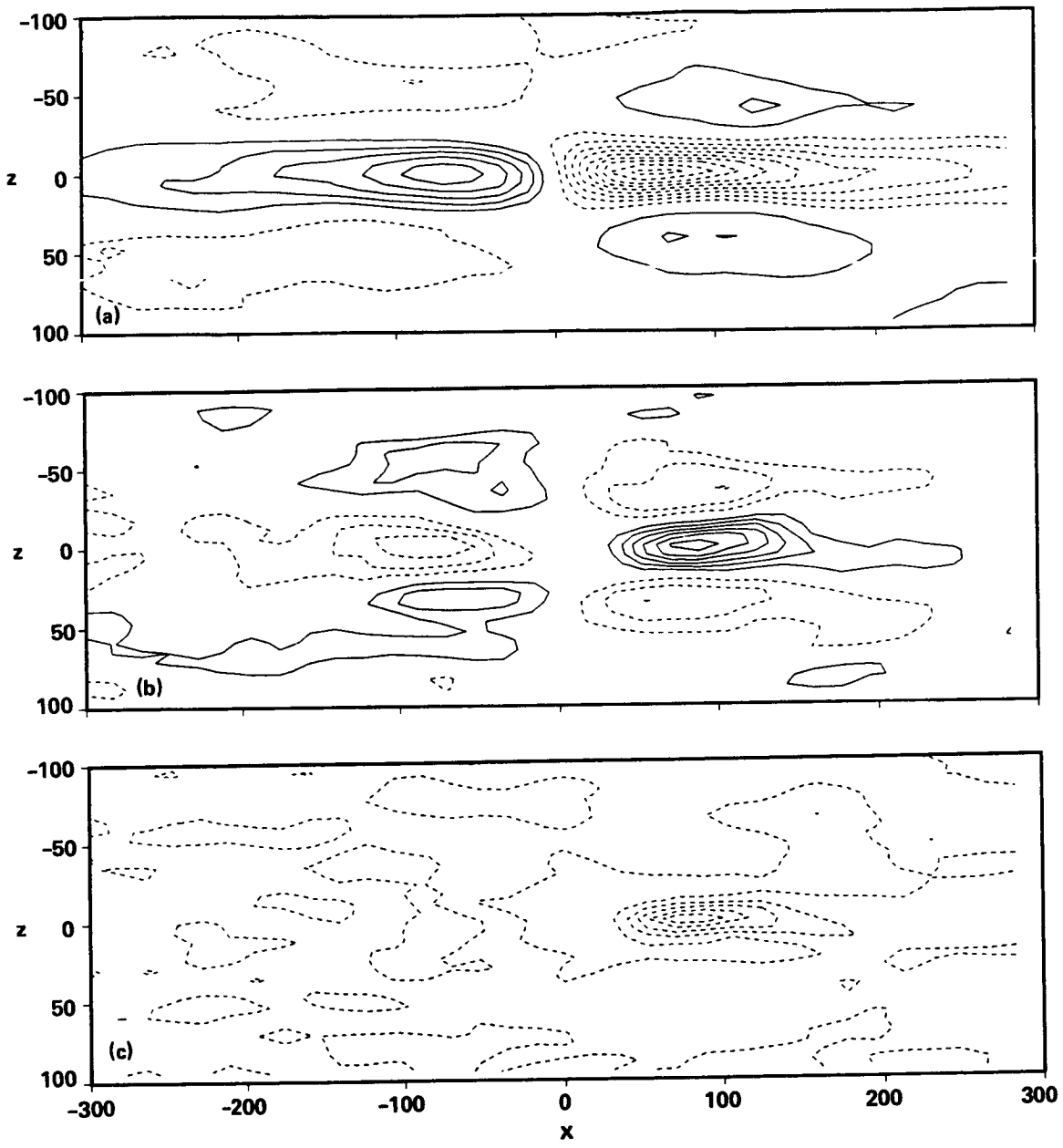

FIGURE 8. Contours in the (x, z)-plane at y=15 of the conditionally averaged shear layer structure. Detection parameters: L=200 and k=1 (same data as in Fig. 7). (a) $< u >$, contour increment is 0.5. (b) $< v >$, contour increment is 0.1. (c) $< uv >$, contour increment is 0.5.

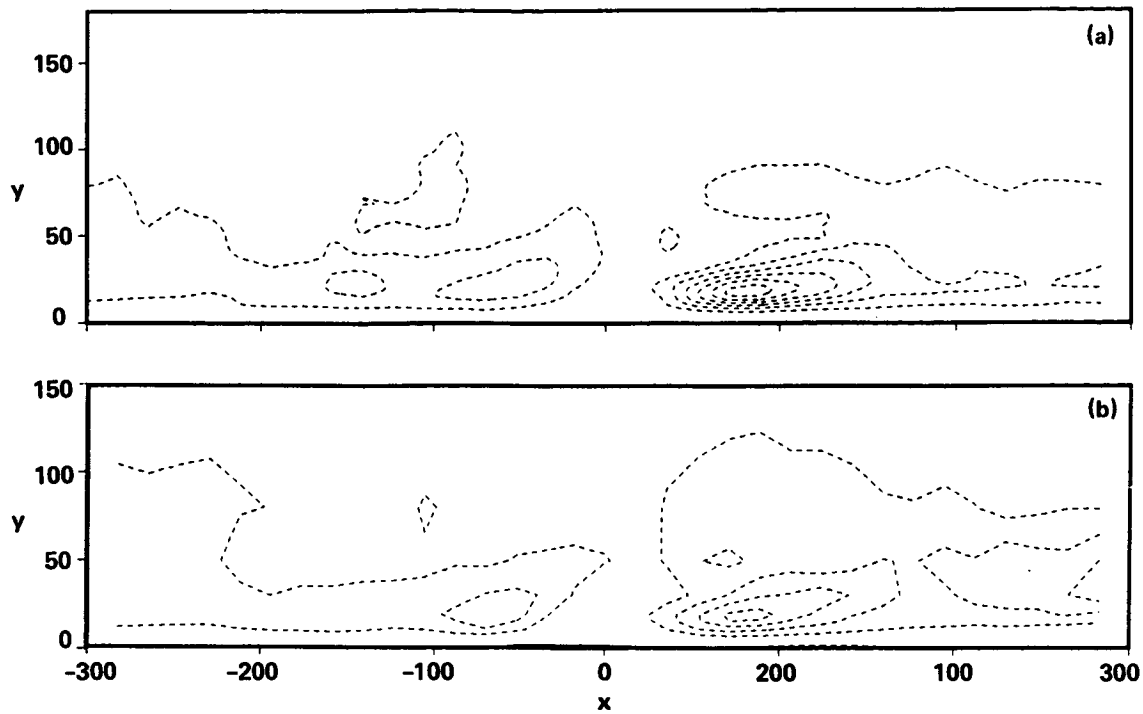

FIGURE 9. Conditionally averaged uv (L=200, k=1, contour increment is 0.5). (a) with alignment in spanwise direction (b) without alignment.

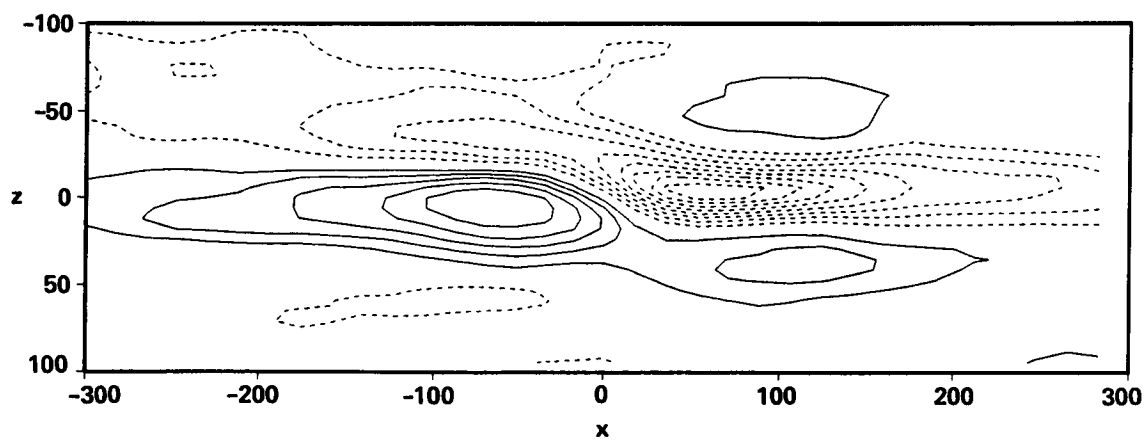

FIGURE 10. Conditionally average ($< u >$) detected with the VISA-criterion (L=200 and k=1) and the asymmetry condition (same data as in Fig. 8a). Data is at y=15 and contour increment is 0.5.

through spanwise motions of the high- and low-velocity regions. Such gradients play a relatively important role for the generation of conditionally averaged turbulence production (as will be discussed below).

The often occurring asymmetric features of the shear layers are illustrated by the space-time development of a single event in Fig. 11, where the frame of reference is chosen so that the center of the shear layer is stationary. The xy- plane view clearly shows the sharpening of the shear layer due to the action of the mean shear, whereas the planar view illustrates a meandering of the high- and low-speed regions, resulting in steep streamwise and spanwise gradients.

A key issue for the importance of coherent structures in turbulent flows is their role in the turbulence-production process. One can show that the conditionally averaged production of turbulent kinetic energy for a plane two-dimensional flow can be written as

$$\begin{aligned} < P > = & - < uv > \frac{dU}{dy} - \overline{u^2} < \frac{\partial u}{\partial x} > - \overline{uv}(< \frac{\partial u}{\partial y} > + < \frac{\partial v}{\partial x} >) \\ & - \overline{v^2} < \frac{\partial v}{\partial y} > - \overline{w^2} < \frac{\partial w}{\partial z} > . \end{aligned} \tag{1}$$

The only term that remains in the long-time-averaged sense is $< uv > dU/dy$. However, the total conditionally averaged production (Fig. 12a) is substantially higher than what can be accounted for by this term (Fig. 12b). This is mainly due to strong gradients in the x- and y-directions of the conditionally averaged streamwise velocity (Fig. 12c). The largest of these terms is the second term in Eq. (1), which is illustrated in Fig. 13 where the production terms have been averaged over an area of 300×40 (streamwise and spanwise extent, respectively). Integrating the conditional production out to $y = 30$ gives an average over this volume which is almost twice as large as the long- time mean value. Moreover, the dissipation of turbulence energy is large in the vicinity of the shear layer (Fig. 14). It is noteworthy here that the conditionally averaged $\partial u/\partial z$ does not enter the left-hand-side expression of Eq. (1). Hence, although there exist high values of the spanwise gradient of u at the edges of the shear layers, they do not in themselves imply contributions to the associated turbulence production.

3. Boundary-layer results

Computer-generated data bases for a turbulent boundary-layer flow at two different Reynolds numbers were also analyzed. These data bases are described in detail in Spalart (1987). In order to investigate whether the size of the near-wall structures shows any significant Reynolds number variation, the ensemble-averaging procedure was carried out for momentum-thickness Reynolds numbers (Re_θ) of 670 and 1410 (Figs. 15a,b). One may note that the structure is somewhat larger in terms of viscous units for the higher Reynolds number, especially on the sweep side. This Reynolds number dependence indicates that there is some influence of the outer flow on the scale of inner-layer structures, and hence some interaction between the outer and inner regions of the flow. However, the influence is rather weak, and the structures are mainly determined by the conditions at the wall.

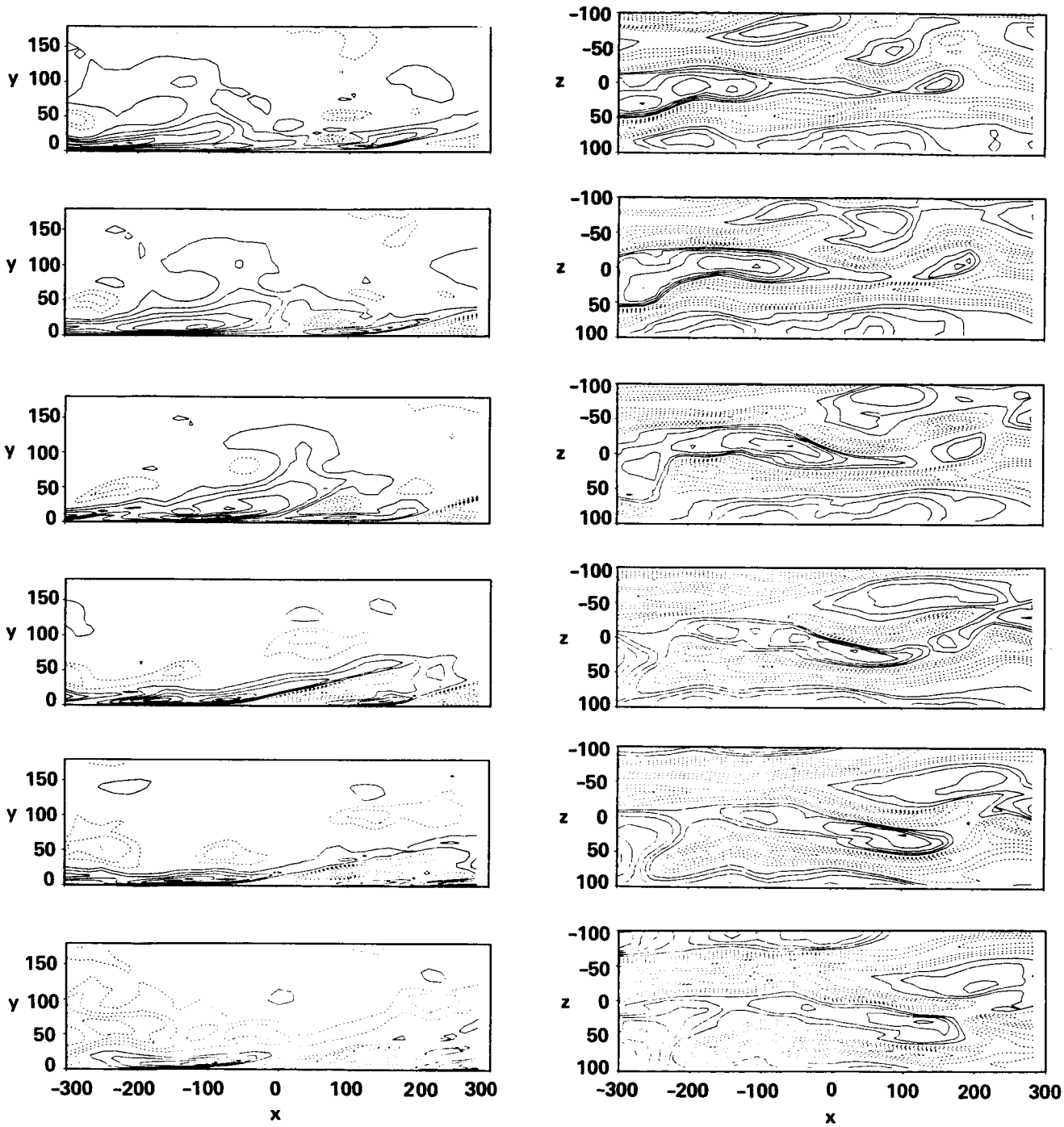

FIGURE 11. (x, y)- and (x, z)-plane of event B in Fig, 1 followed in time. Time increment between plots is 12 viscous units.

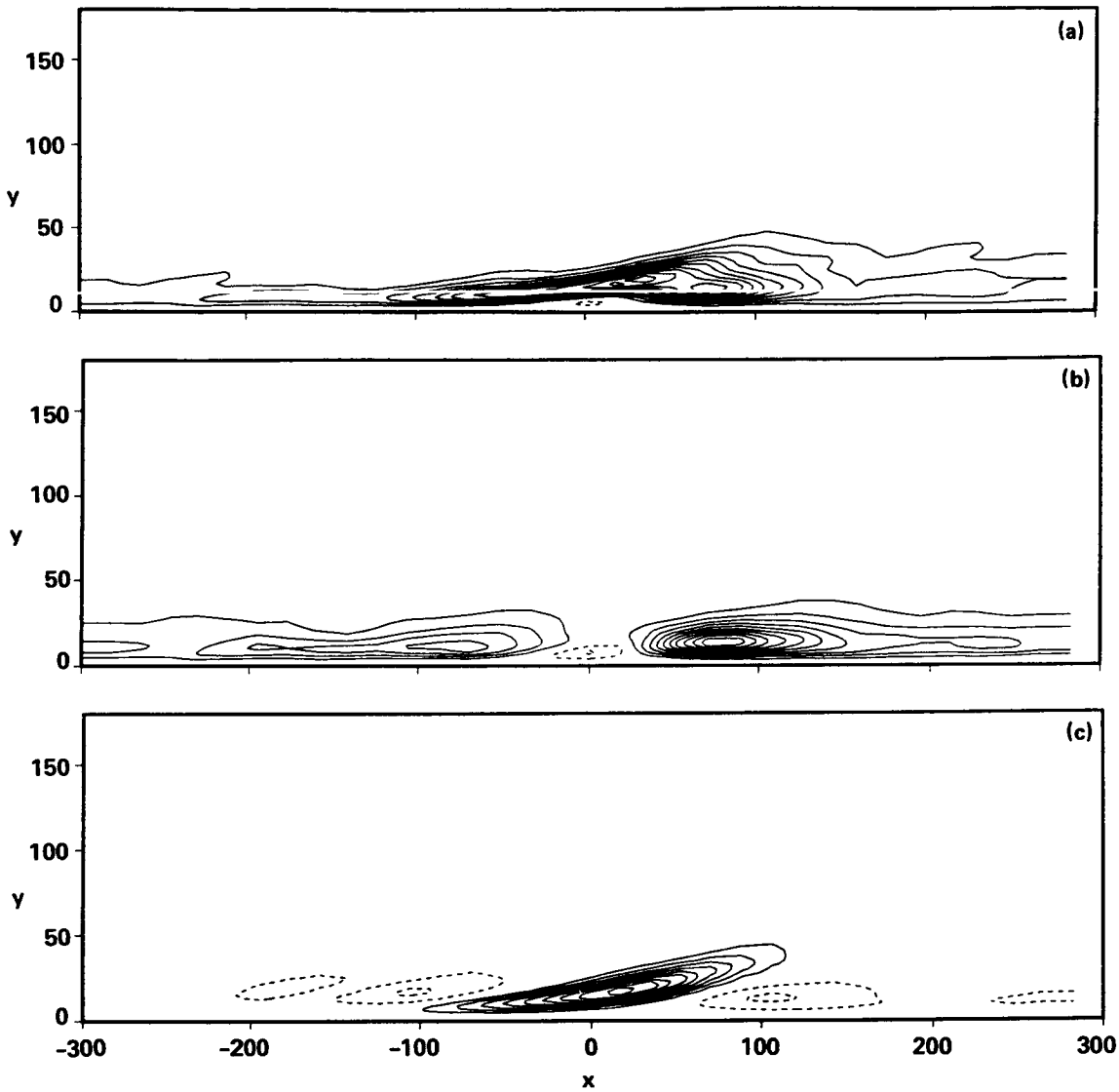

FIGURE 12. Energy production in the symmetry plane of the shear layer (contour increment is 0.1). (a) Total conditional averaged production $< P >$. (b) Reynods-stress induced production $< -uv > dU/dy$. (c) $< P >$ - $< -uv > dU/dy$.

4. Conclusions

- Shear-layer structures are found frequently in near-wall turbulence and often have many features in common with the conditionally averaged structure obtained with the VITA or VISA methods.
- Coherent shear-layer structures in the near- wall region ($y^+ < 15$) were found to propagate with a velocity of about $10.6u_\tau$, and retained their coherence over streamwise distances on the order of a thousand viscous length units.
- Shear-layer structures were found to be important contributors to the turbulence production, and a substantial part of the conditionally averaged production was

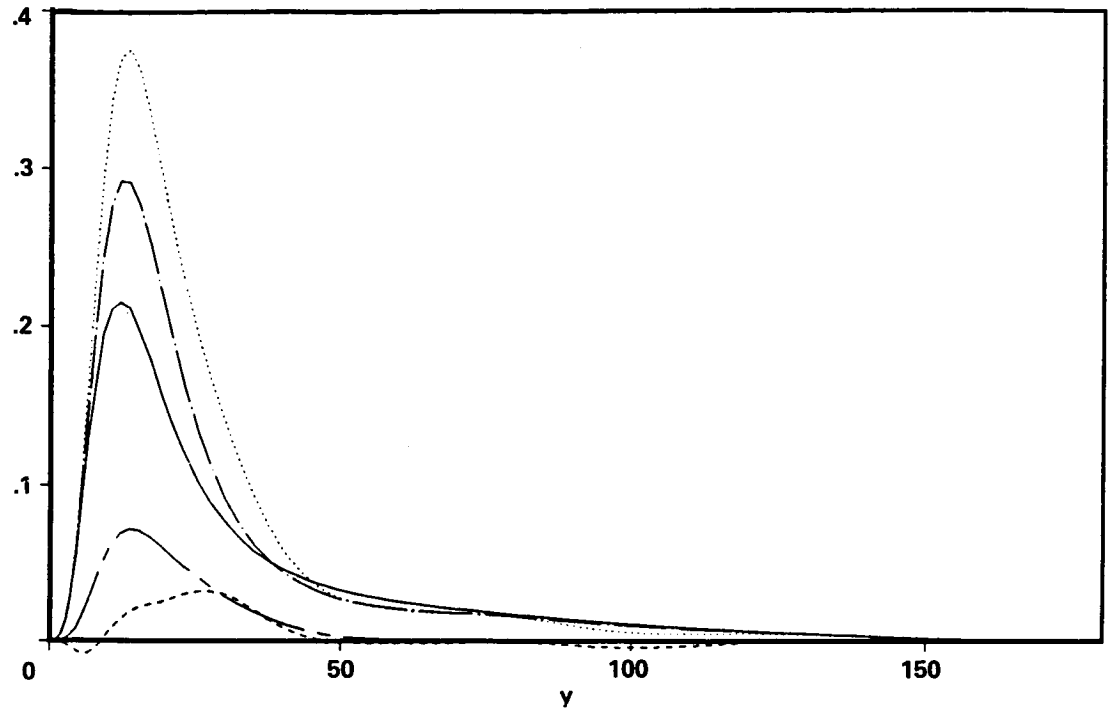

FIGURE 13. Energy production averaged over area around center of event: ——, $-\overline{uv}dU/dy$; ····· , $< P >$; - - - - $-\overline{uv} < \partial u/\partial y >$; — · —, $- < uv > dU/dy$; chndsh $-\overline{u^2} < \partial u/\partial x >$.

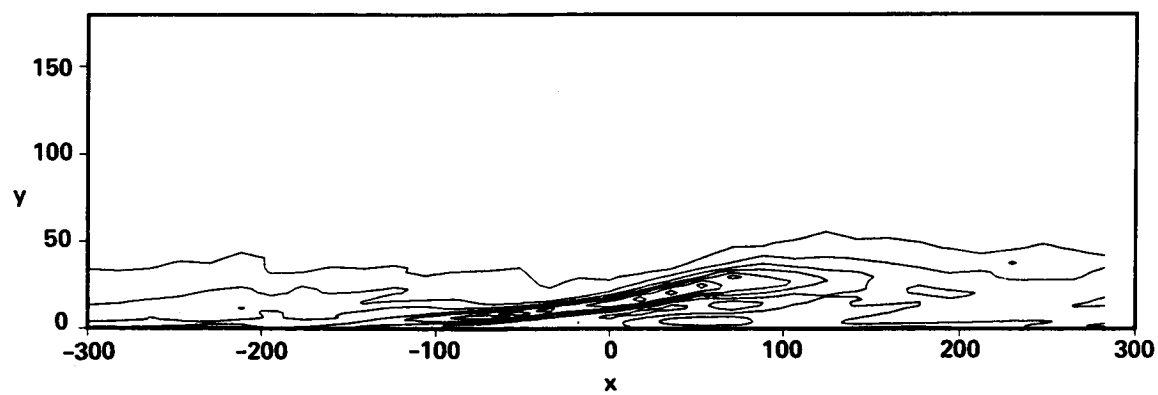

FIGURE 14. Dissipation of turbulent energy in the symmetry plane of the conditional averaged structure in Fig. 7. Contour increment is 0.1.

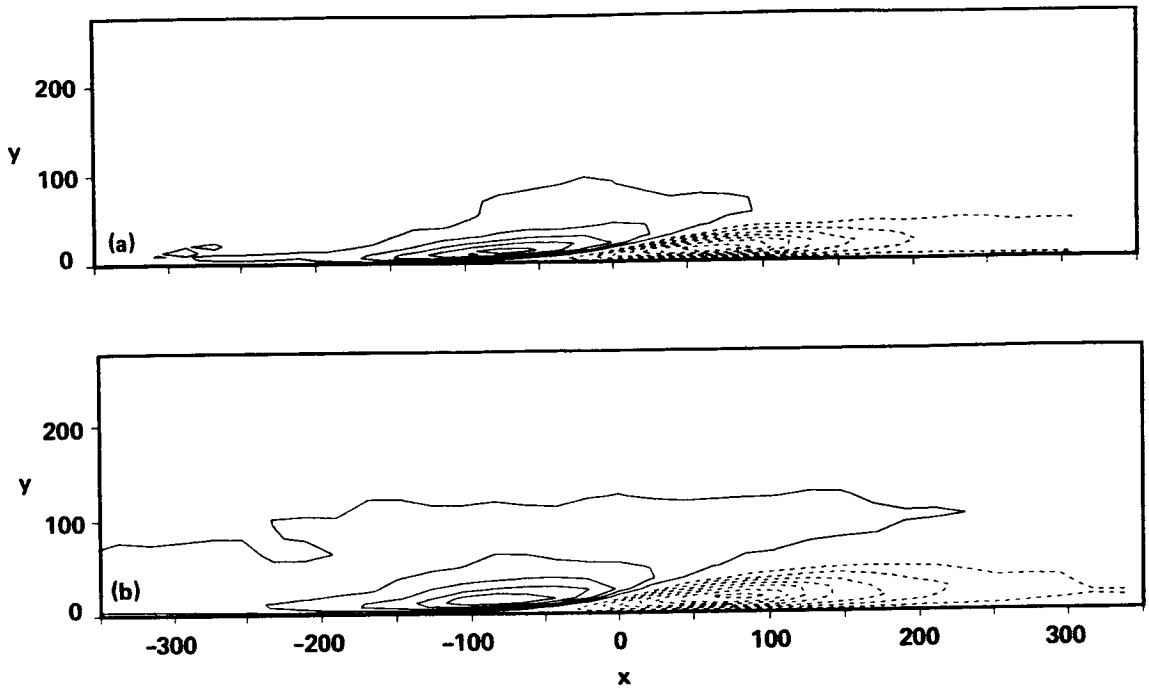

FIGURE 15. Conditionally averaged u obtained from boundary layer simulations (k=1): (a) Re_θ=670, L=211; (b) Re_θ=1410, L=232.

shown to be generated by strong gradients in the streamwise disturbance velocity.

- The dominant associated uv-contribution was found to be associated with an ejection type of motion on the downstream side of the shear layer.
- Individual shear layers often develop a strong asymmetry (which is lost in conventional averaging procedures) as they propagate downstream.

We are grateful to Dan Henningson for much valuable assistance with the computers and many lively discussions. We also wish to thank Philippe Spalart for providing the boundary-layer data, and Kenny Breuer and Marten Landahl for many fruitful discussions.

REFERENCES

ALFREDSSON, P. H., & JOHANSSON, A. V. 1984 Time scales in turbulent channel flow. *Phys. Fluids.* **27,** 1974.

BLACKWELDER, R. F., & KAPLAN, R. E. 1976 On the wall structure of the turbulent boundary layer. *J. Fluid Mech..* **76,** 89.

JOHANSSON, A. V., & ALFREDSSON, P. H. 1982 On the structure of turbulent channel flow. *J. Fluid Mech..* **122,** 295.

JOHANSSON, A. V., ALFREDSSON, P. H., & ECKELMANN, H. 1987 On the evolution of shear-layer structures in near- wall turbulence. in *Advances in Turbulence* (G. Comte-Bellot and J. Mathieu, eds.), Springer-Verlag.

KIM, J. 1985 Turbulence structures associated with the bursting event. *Phys. Fluids.* **28,** 52.

SPALART, P. 1987 Direct simulation of a turbulent boundary layer up to R_θ = 1410. NASA Technical Memorandum 89407.